Linear Barotropic Instability of the Tropical Easterly Jet on a Sphere

S. K. MISHRA

Indian Institute of Tropical Meteorology, Pune—411 005, India

(Manuscript received 26 November 1985, in final form 5 August 1986)

ABSTRACT

A barotropic global spectral model is used to determine the linear divergent barotropic instability characteristics of the tropical easterly jet by applying an initial value technique. These characteristics are compared with those on a beta plane, in order to identify the important effects of the spherical geometry on unstable modes. The increase in the growth rate of unstable modes on the sphere is due to the absence of lateral walls. The primary and secondary maxima of the wave amplitude are located at 3.5° and 18.5°N, respectively. It is found that the spherical geometry plays an important role in locating the wave amplitude maximum and the angular momentum transports by the wave. There exists a strong correlation between the two wave amplitude maxima and the extrema of $\bar{q}_\mu/a$ and $\bar{q}$.

It is seen that the midlatitude westerly jets stabilize the easterly jet. The influence of westerly jets is investigated in terms of the overreflection of the meridional propagation of waves from critical latitudes.

1. Introduction

Manabe et al. (1970) have concluded by comparing the eddy kinetic energy spectra obtained from their dry and moist tropical simulation experiments that the characteristic scale of the upper tropospheric disturbances is controlled mainly by other than the moist processes. They have also noted that the moist process increases the amplitude of the upper tropospheric disturbances. This amplitude increase may be due partly to the enhanced interactions between the planetary and synoptic-scale waves that are observed in the tropics during the northern summer (Kanamitsu et al., 1972). Further evidence in support of the view that the development of synoptic-scale upper tropospheric disturbances is due mainly to the adiabatic processes is provided by the results of a nondivergent barotropic simulation experiment performed by Colton (1973). He was able to simulate many observed features of synoptic-scale disturbances in the vicinity of the easterly jet at 200 mb. It is also recognized that the CISK process cannot explain the scale of tropical disturbances (Chang, 1971). Hence, the effect of cumulus convection is not considered in this study.

Many investigators have performed barotropic, baroclinic and combined barotropic–baroclinic stability analyses of the observed and idealized easterly jets (Shukla, 1977; Tupaz et al., 1978; Mishra and Salvekar, 1980; Mishra et al., 1981; Mishra and Tandon, 1983) by using linear, quasi-geostrophic models on a beta plane.

Hollingsworth (1976), Moura and Stone (1976), Simmons and Hoskins (1976) and others have investigated the effects of spherical geometry on baroclinic instability of midlatitude westerly flows. In this study, we intend to investigate the properties of the barotropic unstable modes of the tropical easterly jet on the sphere and the influence on them by the midlatitude westerly jets of the Northern and Southern hemispheres. For this purpose, even though it is known that the ageostrophic effects are likely to be significant for the disturbances as they are observed very close to the equator (Krishnamurti, 1971), we still choose to perform the numerical calculations by using the quasi-geostrophic barotropic model because it will be easier to understand the effects of the earth's spherical geometry in this model than in a primitive equation model.

2. Model and system of equations

a. Linear model

We consider the horizontal motions on the surface of a sphere of radius a, which is rotating with an angular speed ω around its vertical axis. It is well known that the upper tropospheric disturbances in the vicinity of the easterly jet rarely extend downward to the lower troposphere. Further, it is theoretically established that the waves are vertically trapped by easterlies (Charney and Drazin, 1961). It is an observed fact that in the tropics the tropopause ($\sim$100 mb) is capped by a very stable inversion layer. In view of these facts, for incorporating the effect of divergence and vertical density stratification on the motions, a gravitationally stable three-layer system is considered. Each layer of the system is homogeneous, incompressible, inviscid, nonmixing, barotopic and in hydrostatic balance. The top and bottom layers are kept at rest and the motion in the middle layer is quasi-geostrophic.

The linear potential vorticity equation, which governs the motion of an infinitesimally small perturbation superposed on the basic state zonal wind $\bar{u}(\mu)$, can be written as

$$q_t + \bar{U}q_\lambda/[a(1-\mu^2)] + \bar{q}_\mu\psi_\lambda/a^2 = 0, \quad (1a)$$

where

$$q = \nabla^2\psi - R_e^{-2}\psi, \quad (1b)$$

$$\bar{q}_\mu/a = (2\Omega - \bar{U}_{\mu\mu}/a)/a + R_e^{-2}\bar{U}/(1-\mu^2), \quad (1c)$$

$$R_e = (a^2 g^* H/4\Omega^2)^{1/4}, \quad (1d)$$

$$g^* = g(\theta_3-\theta_2)(\theta_2-\theta_1)/[\theta_2(\theta_3-\theta_1)], \quad (1e)$$

$$\bar{U} = \bar{u}\cos\varphi, \quad (1f)$$

$$\mu = \sin\varphi. \quad (1g)$$

Here the overbar symbol denotes the basic state (zonal average) quantities, ψ is the perturbation streamfunction, q the potential vorticity, φ the latitude, R_e the equatorial Rossby radius of deformation, g^* the reduced gravity, and H the constant thickness of the middle layer. The symbols θ_1, θ_2 and θ_3 are the vertically averaged potential temperatures of bottom, middle and top layers, respectively.

Equation (1d) for the equatorial Rossby radius of deformation is obtained by expressing f_0 as $(2\Omega/a)R_e$ for the equatorial motions in $R_e = (g^*H)^{1/2}/f_0$ (Pedlosky, 1979). For the upper tropospheric disturbances in the vicinity of the easterly jet, the appropriate values for g^* and H are 0.786 m s^{-2} and 9 km, respectively (Mishra et al., 1981). The equatorial Rossby radius of deformation as computed from Eq. (1d) is 1900 km.

b. Kinetic energy equation

The zonally averaged wave kinetic energy equation is obtained from Eq. (1a), which can be written as

$$(K_w)_t = C(K_b, K_w) + \text{HKWC} - R_e^{-2}\bar{\psi}_t^2/2, \quad (2a)$$

where

$$K = \overline{\nabla\psi\cdot\nabla\psi}/2, \quad (2b)$$

$$C(K_b, K_w) = \bar{U}(\overline{UV})_\mu/[a(1-\mu^2)], \quad (2c)$$

$$\text{HKWC} = \overline{[\psi(1-\mu^2)\psi_{t\mu}]}_\mu/a^2. \quad (2d)$$

Here K_w is the wave kinetic energy, $R_e^{-2}\overline{\psi_t^2}/2$ is a form of the wave potential energy associated with the divergence, $C(K_b, K_w)$ denotes the barotropic energy conversion from the basic state kinetic energy (K_b) to the wave kinetic energy, and HKWC denotes the wave kinetic energy convergence. The values of U and V are given by

$$U = -\cos\varphi\psi_\varphi/a, \quad V = \psi_\lambda/a.$$

c. Necessary condition for instability

Lipps (1963) derived the necessary condition for divergent barotropic instability on a beta plane. The necessary condition using the normal model approach in the case of a zonal flow over the sphere can be easily derived from the linear potential vorticity equation [Eq. (1a)] by following the well-known procedure of integral techniques of Rayleigh (1880). The necessary condition for the divergent barotropic instability demands that the basic state potential vorticity gradient, $\bar{q}_\mu/a$, should change sign somewhere within the flow. It can be concluded from the expression for $\bar{q}_\mu/a$ that the divergence effect is likely to destabilize easterly flows and to stabilize westerly flows.

d. Numerical procedure

A nonlinear, quasi-geostrophic, barotropic global spectral model, which includes the divergence term, is adopted for this study. The streamfunction is expanded in truncated series of spherical harmonics in the form

$$\psi(\lambda, \mu, t) = \sum_{m=-M}^{M}\sum_{n=|m|}^{m+J}\psi_n^m(t)P_n^m(\mu)e^{im\lambda}, \quad (3)$$

where $P_n^m(\mu)$ is the associated Legendre function, m the zonal wavenumber, $n - |m| + 1$ a pseudolatitudinal wavenumber, n the total wavenumber, and M and J are the orders of truncation of the series in m and n, respectively. The spectral representation of the nonlinear terms is obtained by utilizing a half-transform method (Eliasen et al., 1970) instead of a full-transform method (Eliasen et al., 1970; Orszag, 1970), which is less efficient than the former for low-resolution integrations of the model (Mishra, 1981). In a linear instability study only two zonal wavenumbers are involved.

The modified Euler-backward time-differencing scheme is used for the first time step, and the leapfrog scheme is used for subsequent time steps, with a time step of 60 min. A time filter as suggested by Robert (1966) is also used for damping temporal oscillations during the integration, which arise due to the noncoupling of the odd and even time steps. The time filter parameter value was 0.01 (Simmons and Hoskins, 1976).

The model is integrated for given non-zero wavenumber m, and it is also ensured that the basic zonal current (wavenumber 0) remains unchanged and that no wave other than the wavenumber m is generated due to nonlinear interactions during the course of integration.

e. Refractive index

On substituting the neutral propagating plane wave solution

$$\psi(\lambda, \mu, t) = \psi(\mu)e^{im(\lambda-\omega_r t)}$$

in Eq. (1a), we obtain

$$[(1-\mu^2)\psi_{\mu\mu}] + \left[\frac{2\Omega - \bar{U}_{\mu\mu}/a + \omega_r a^2 R_e^{-2}}{\bar{\omega}-\omega_r} - \frac{m^2}{1-\mu^2}\right]\psi = 0 \quad (4)$$

where the basic state angular velocity is $\bar{\omega} = \bar{u}/a\cos\varphi$, and ω_r is the real part of complex ω. We define a new independent variable as

$$s = \ln\left[\frac{1+\mu}{(1-\mu^2)^{1/2}}\right] \tag{5}$$

(Bronstator, 1983). Equation (4) can then be written as

$$\frac{d^2\Psi}{ds^2} + l^2\Psi = 0, \tag{6a}$$

where

$$l^2 = \frac{(1-\mu^2)[2\Omega - \bar{U}_{\mu\mu}/a + \omega_r a^2 R_e^{-2}]}{\bar{\omega} - \omega_r} - m^2. \tag{6b}$$

Here l^2 can be identified as a refractive index for meridional propagation. The wave propagation requires that $l^2 > 0$ otherwise there is no propagation of the wave. The latitude where $l = 0$ is called the turning latitude.

It can easily be shown from the linear λ-momentum equation for a barotropic homogeneous fluid in spherical coordinates that

$$\overline{pv} = -\rho_0(\bar{\omega} - \omega_r)\overline{uv}a\cos\varphi, \tag{7}$$

where ρ_0 is the basic state density and $\overline{pv}$ denotes the wave energy flux. Equation (7) is derived for propagating neutral waves and its growth is neglected. Thus the equation can be used for weakly unstable modes.

3. Basic zonal flow

The zonal wind profile at 100 mb between 10°S and 30°N is constructed by averaging the observed mean June–August zonal wind in the interval 55°–105°E. For the easterly jet (EJ) profile, the wind outside this latitude interval is assumed to approach zero exponentially. In order to investigate the influence of the midlatitude westerly jets of the Northern and Southern hemispheres on the unstable modes, the full (F) profile is obtained by using the zonal average mean wind outside the interval 10°S–30°N. The profiles are fitted by truncated Legendre series for $J = 20$. In the latitude interval 10°S–30°N, the fitted profiles are able to explain more than 99% of the observed variance. The fitted EJ and F profiles of $\bar{U}$ ($=\bar{u}\cos\varphi$) are presented in Fig. 1. The differences between two fitted profiles in the interval 10°S–30°N cannot be resolved in the figure because the maximum absolute difference between them was less than 0.4 m s^{-1}.

In Fig. 2 is illustrated $\bar{q}_\mu/a$ for the easterly jet; $\bar{q}_\mu/a$ for the full profile was also computed but not presented because the westerly jets do not satisfy the necessary condition for instability. It is seen from the figure that the easterly jet satisfies the necessary condition for divergent barotropic instability over the sphere. It may be noted that the necessary condition for the nondivergent case is also satisfied.

4. Results for the EJ profile

For obtaining the numerical solutions corresponding to the fastest growing mode, the model is integrated with a truncation $J = 20$. The initial conditions consist of a wave of given wavenumber m having a small amplitude and superposed on the basic zonal current. The kinetic energy sprectrum of the initial wave is uniform with respect to the total wavenumber n. The model integration was terminated when the wave reached a state of uniform exponential growth. For this purpose, we have adopted the following procedure. First, we have ensured that the relative error between two con-

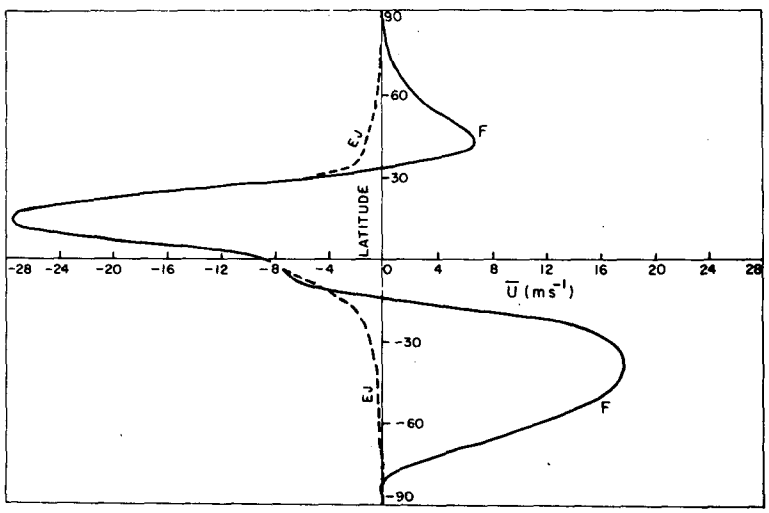

FIG. 1. Meridional profiles of longitudinally averaged (55°–105°E) zonal wind (m s^{-1}) for the easterly jet (EJ) and for the global case (F).

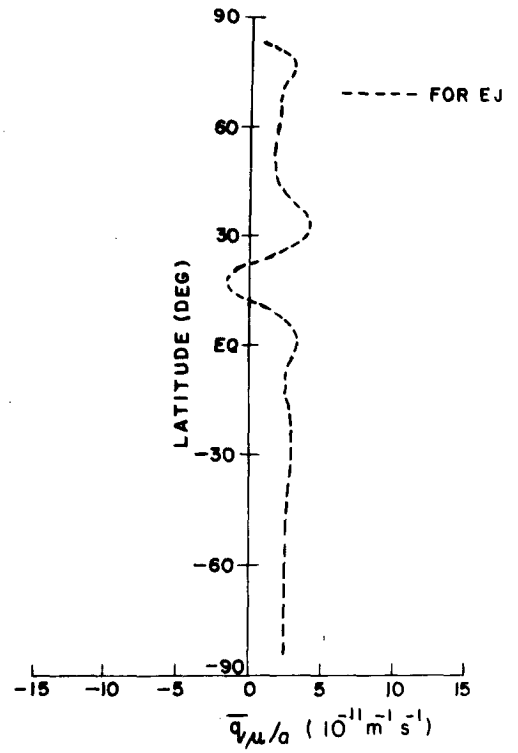

FIG. 2. Meridional profile of the meridional gradient of basic state potential vorticity, $\bar{q}_\mu/a$ (10^{-11} m^{-1} s^{-1}), for the EJ basic state.

secutive six-hourly averaged growth rates of the wave is less than a prespecified value (10^{-3}). Next, we have demanded that the relative errors between the growth rates of different meridional modes of the growing wave are less than the prespecified value. This final criterion has ensured that the growth rate spectrum with respect to n is uniform to a good degree of accuracy. It is easily understood that the different meridional modes of the exponentially growing wave should have the same growth rates.

a. Growth rate and phase speed spectra

The growth rate and phase speed as a function of zonal wavenumber m for the divergent and nondi-vergent cases of EJ profile are plotted in Figs. 3a and 3b, respectively. The most unstable divergent wave of zonal wavenumber 7, which corresponds to a wavelength of 5700 km at the equator, has an e-folding time of 3.82 days and a phase speed of -19.9 deg day^{-1}. This value of the preferred wavelength is smaller than that of the beta-plane value. A comparison between the divergent and nondivergent growth rate spectra has indicated that the divergence destabilizes the flow and also shifts the preferred wave toward a longer wavelength. The growth rate increase in the divergence case can easily be understood in terms of the decrease in the effective value of beta due to the divergence. We note that the preferred

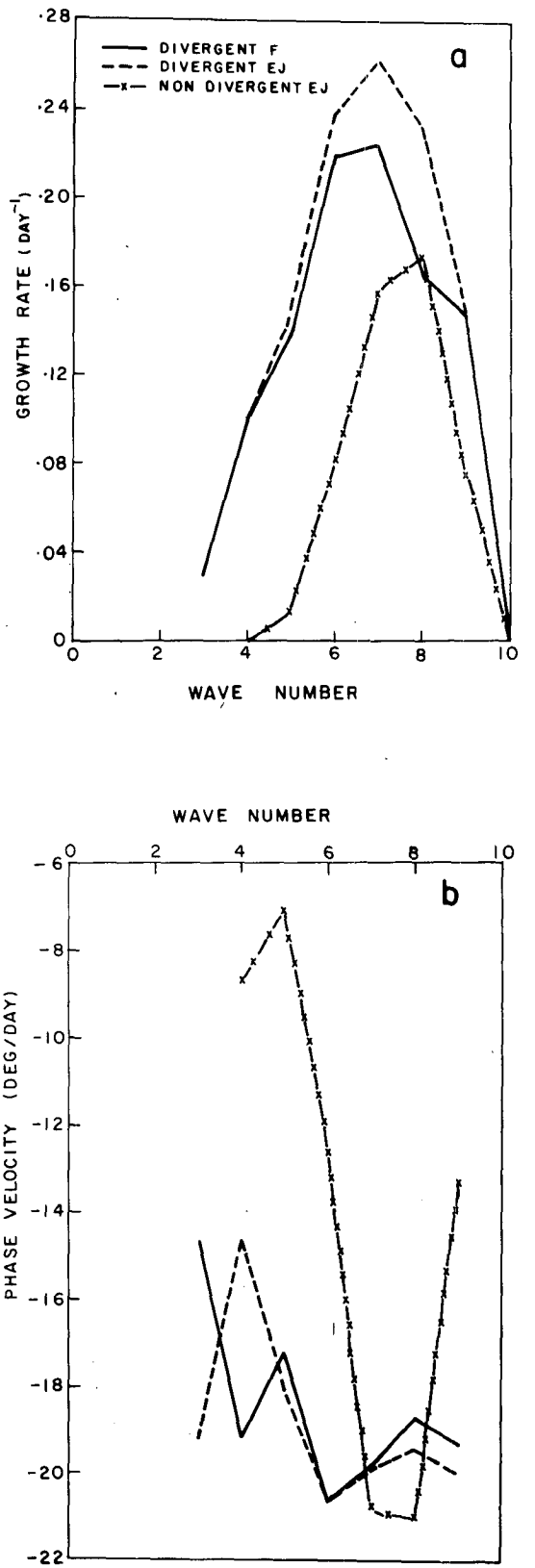

FIG. 3. (a) Growth rate (day^{-1}) and (b) phase speed (deg day^{-1}) for the divergent and nondivergent cases and for the EJ and F profiles.

wave tends to move westward much faster than the observed disturbances (Krishnamurti, 1971). The growth rates obtained on the sphere are much larger than the growth rates obtained by using a quasi-geostrophic, barotropic beta-plane channel model for the easterly jet profile between 4°S and 32°N (Mishra et al., 1981).

The spherical geometry and the absence of lateral walls are the possible causes for the increase in the growth rates and the decrease in the preferred wavelength on the sphere as compared to the beta-plane values. In order to identify the dominating factor between these, growth rate and phase velocity spectra were computed for four different easterly jet profiles with their centers located at 0°, 7.5°, 12.5° and 17.5°N (not presented). In each case the jet was displaced, without any change in the wind distribution with respect to its center, except at latitudes close to the poles. It was noted that the largest difference between the maximum growth rates for the four cases was less than 5%. Furthermore, the preferred wavenumber was not affected by the displacement of the jet center.

The results indicate that the increase in the growth rates and the decrease in the preferred wavelength on the sphere can be attributed to the absence of lateral walls. This conclusion is in agreement with the results obtained by Yamasaki and Wada (1972) in their study on the effect of lateral boundaries on the stability properties of an easterly symmetric jet on a beta plane. They have found that a shift in lateral walls away from the shear zones leads to a significant decrease in the preferred wavelength. Further, they have noticed the presence of antisymmetric modes with significant growth rates as the lateral walls are moved away from the shear zones. In this study no preferred latitude is noticed for the observed tropical easterly jet center, as had been found by Kuo (1978).

b. *Structure*

The streamfunction distribution in the horizontal plane associated with the divergent preferred wave for the EJ profile is computed. The values have been normalized so that the maximum value is ten and the wave phases are also normalized so that the phase at the equator is zero. The streamfunction distribution in the latitude interval 25°S and 40°N is presented in Fig. 4a. Beyond this latitude interval the streamfunction values are found to be small. The wave amplitude profile of the divergent asymmetric preferred wave of wavelength 6500 km as obtained from the beta plane channel model centered at 14°N is presented in Fig. 4b (Mishra et al., 1981). From the distribution it is seen that the wave amplitude has two maxima of comparable magnitudes in the spherical case (Fig. 4a). The primary maximum is located close to the equator at 3.5°N, and the secondary maximum is located at 18.5°N to the north of the jet center (13.75N), while the beta-plane calculations indicate the presence of only one wave amplitude maximum located at 6°N (Fig. 4b). The more southward location of the primary-wave amplitude maximum on the sphere is closer than that of the beta-plane location to the observations (Krishnamurti, 1971) and simulation results (Colton, 1973). The wave has a sharp southwest to northeast tilt with respect to latitude between the primary and secondary amplitude maxima, and the tilt is from southeast to northwest northward of the secondary amplitude maximum. The sudden change in the tilt direction is found to occur at a latitude north of the jet center, whereas in the beta-plane results this change is found to occur at the jet center. From the above discussion, we conclude that the inclusion of the full effect of the rotating spherical earth leads to significant changes in the structure of barotropic unstable waves.

We note that the secondary amplitude maximum is located close to the mean latitude of the summer monsoon trough in the lower troposphere over the Indian region. There is observational evidence for the existence of synoptic-scale upper tropospheric disturbances close to the monsoon trough (Srinivasan, 1960).

It is seen from Figs. 2 and 4a that the primary-wave amplitude maximum lies close to the positive $\bar{q}_\mu/a$ maximum, which is to the south of the easterly jet center. A similar relationship between the wave amplitude and $\bar{q}_\mu/a$ maximum has been found by Mishra et al., (1981) for the barotropic unstable waves on the beta plane. We note that $\bar{q}_\mu/a$ profiles also have another positive maximum of a relatively larger value to the north of the jet center. An examination of the $\bar{q}$ profile (Fig. 5) has indicated that the secondary-wave amplitude maximum lies close to the potential vorticity minimum, as first pointed out by Kuo (1978) for a barotropic unstable flow and subsequently noted by Mak and Kao (1982) for a barotropic, unstable low-level zonal wind over the south central Arabian Sea during the onset of the southwest monsoon.

In order to verify the above relationship, the horizontal structure of the preferred waves and $\bar{q}_\mu/a$ and $\bar{q}$ profiles are computed for the four different latitude locations of the easterly jet center, as has been mentioned earlier. It has been noticed that a latitudinal shift in the location of the $\bar{q}_\mu/a$ maximum was invariably associated with a similar latitudinal shift in the location of the primary-wave amplitude maximum. A similar association between the shift of $\bar{q}$ minimum and the location of secondary amplitude maximum was also noticed.

The meridional scale of the easterly jet determined as the meridional distance over which the zonal wind is equal to or more than half of its maximum value (half-width) is found to be 2600 km (Fig. 1). The meridional scales for the preferred waves on the sphere and beta plane as determined from their amplitude profiles (Figs. 8 and 4b) are 4750 and 1600 km, respectively. A comparison between the two profiles fur-

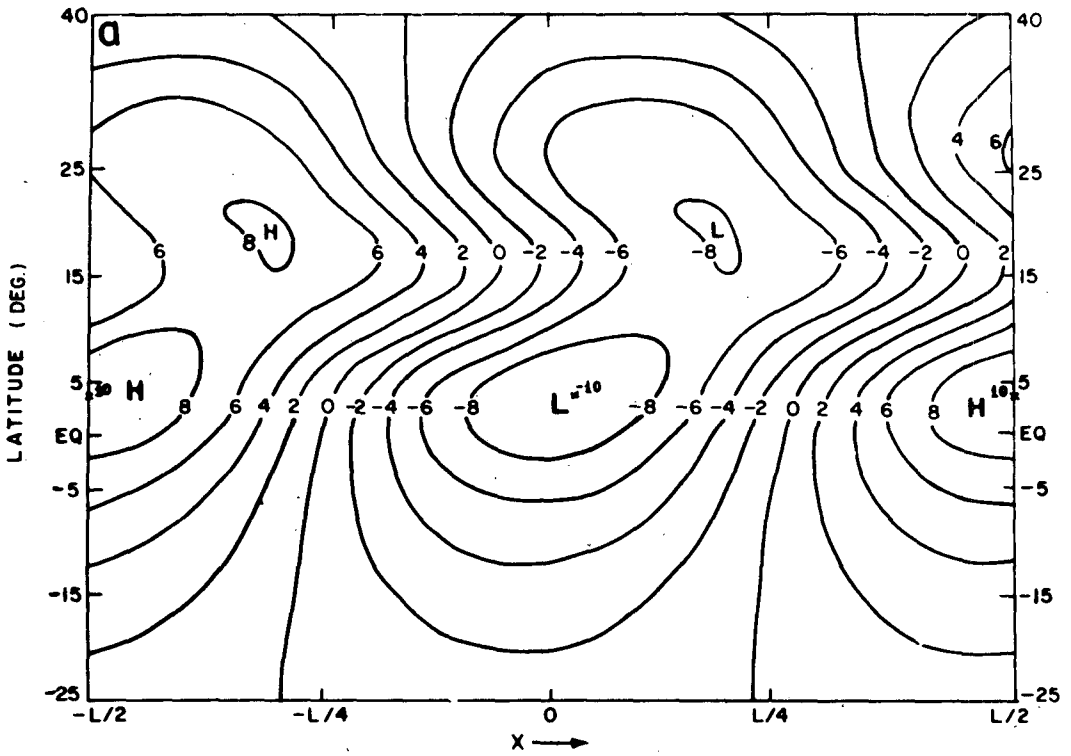

FIG. 4. (a) Horizontal plane distribution of streamfunction for the divergent preferred wave of wavenumber 7 on the sphere for the EJ basic state. (b) Wave amplitude profile of the divergent asymmetric preferred wave on the beta plane. The maximum value is normalized to ten in both cases.

ther indicates that the large meridional scale of the preferred wave on the sphere in comparison to the beta-plane wave is mainly associated with the large asymmetry around the amplitude maximum, which in turn is due to a considerably slower decrease of amplitude to the north of its maximum in the former than the latter case. In view of this fact and the fact that the amplitude maximum is located closer to the southern boundary in the beta-plane case, we conclude that the increase in the meridional scale of the preferred wave on the sphere is mainly due to the spherical geometry and not to the absence of lateral walls. Here is an example of an unstable mode having a meridional scale larger than the meridional scale of the basic state and the Rossby radius of deformation.

c. *Zonal angular momentum transport*

The zonal angular momentum transport, $\overline{UV}$, profile is computed for the normalized preferred wave with a maximum meridional wind of 6 m s^{-1} (Krishnamurti, 1971) and is presented in Fig. 6a. The momentum transport ($\overline{u'v'}$) profile for the beta-plane divergent asymmetric preferred wave, also normalized to a maximum meridional wind of 6 m s^{-1}, is given in Fig. 6b. It is seen from Fig. 6a that the easterly angular momentum transports are southward from 15°S to 17°N and northward beyond 17°N. Furthermore, the transport reached a maximum value at 10°N while the jet center was located at 13.75°N. The transports near the jet center in the spherical case are significantly more than the values for the beta-plane case. It is found that the location of maximum southward easterly momentum transport coincides with the location of largest meridional wind shear associated with the easterly jet. Recent baroclinic instability studies for midlatitude westerly flows have shown that the inclusion of the full effect of the rotating spherical earth has resulted in displacing the computed momentum transport maximum to the westerly jet center (Hollingsworth, 1975; Simmons and Hoskins, 1976). In the present study a shift is noticed in the momentum transport maximum toward the jet center as an effect of the spherically rotating earth. It may be noted that the momentum transport maximum for a nondivergent wave of wavenumber 8 is located at 12.5°N, which is very close to the jet center.

d. *Barotropic energy conversion*

It can be concluded from Fig. 7a, which contains the meridional profiles of the barotropic energy conversion, $C(K_b, K_w)$, and the horizontal wave kinetic energy convergence (HKWC) associated with the normalized preferred wave, that the wave receives the ki-

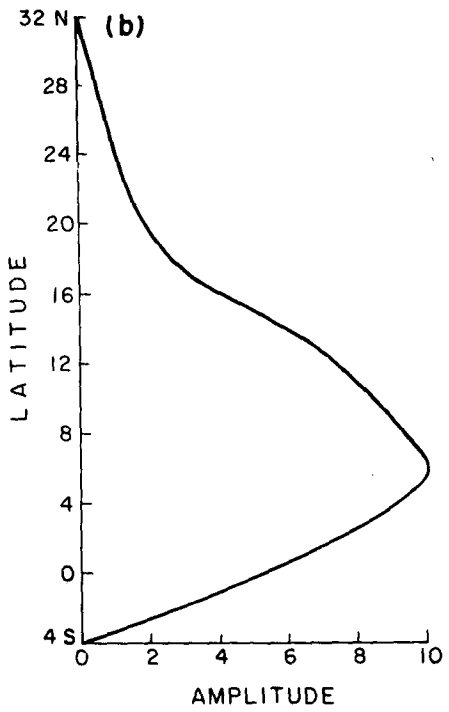

FIG. 4. (*Continued*)

netic energy from the basic zonal flow in a narrow zone around the jet center. Away from the center the wave gains the kinetic energy through the process of the horizontal wave kinetic energy convergence. The $C(K_b, K_w)$ and HKWC profiles are very nearly symmetric with respect to the jet center, while in the case of beta-plane waves the profiles are quite asymmetric with the maximum energy conversion occurring to the south of the jet center (Fig. 7b). The latitude interval where the wave is gaining the kinetic energy from the basic flow is nearly twice as large as the interval found in the beta-plane case. Further, the positive energy conversion values in the former case are nearly three times that of the latter case. This is consistent with the results that the growth rate and the wave meridional scale on the sphere are larger than the corresponding values on the beta plane.

5. Influence of midlatitude westerly jets

A comparison between the growth rate spectra for the F and EJ profiles (Fig. 3a) indicates that the Northern and Southern hemispheric midlatitude westerly jets inhibit the growth of disturbances along the tropical easterly jet. It may be added that the growth rate spectra were also computed for the basic state $\bar{u}$ profiles obtained after removing one of the westerly jets at a time (results not presented). It was concluded from these computations that the stabilizing influence of the northern westerly jet dominates over that of the southern westerly jet.

Figure 8 shows the amplitude distribution of the preferred wave for the F and EJ basic zonal wind profiles. It is concluded that the presence of westerly jets leads to the decrease of the meridional scale of wave, and, in this connection, the effect of the northern westerly jet is more pronounced than that of the southern westerly jet.

In order to understand the nonlocal influence of westerly jets in terms of the meridional propagation of the wave and its interaction with the basic state at the critical latitudes, the refractive index square (l^2) is computed on the grid interval of 2.5° for the two cases. The results of these computations are presented in Figs. 9a and 9b. For the two cases, the critical latitudes where $\bar{\omega} = \omega_r$ are computed, and the turning latitudes where $l^2 = 0$ as obtained from l^2 profiles are shown in Table 1. The critical latitudes to the north and south of the easterly jet center are denoted by CLN and CLS, respectively. It is noted that there exist at least two turning points, one to the north of CLN and the other to the south of CLS. Since $(\bar{\omega} - \omega_r) > 0$ beyond these points, by using the angular momentum flux profile (Fig. 6a) and Eq. (8), it is inferred that the wave energy flux is southward in the region south of CLS and northward to the north of CLN. In the zone between CLS and CLN the wave energy flux is directed toward the latitude where $\overline{UV} = 0$. Thus, southward- (northward) propagating waves dominate in the region south (north) of CLS (CLN). Further, it is inferred that the wave energy flux is directed away from the critical latitudes.

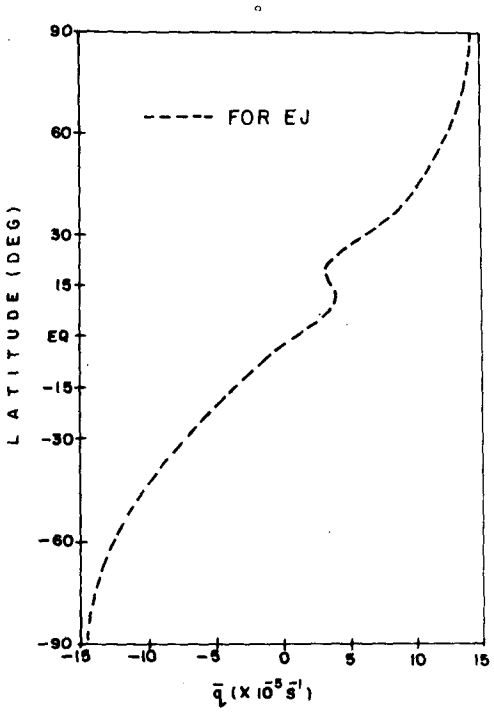

FIG. 5. Meridional profile of $\bar{q}$ (10^{-5} s^{-1}) for the EJ basic state.

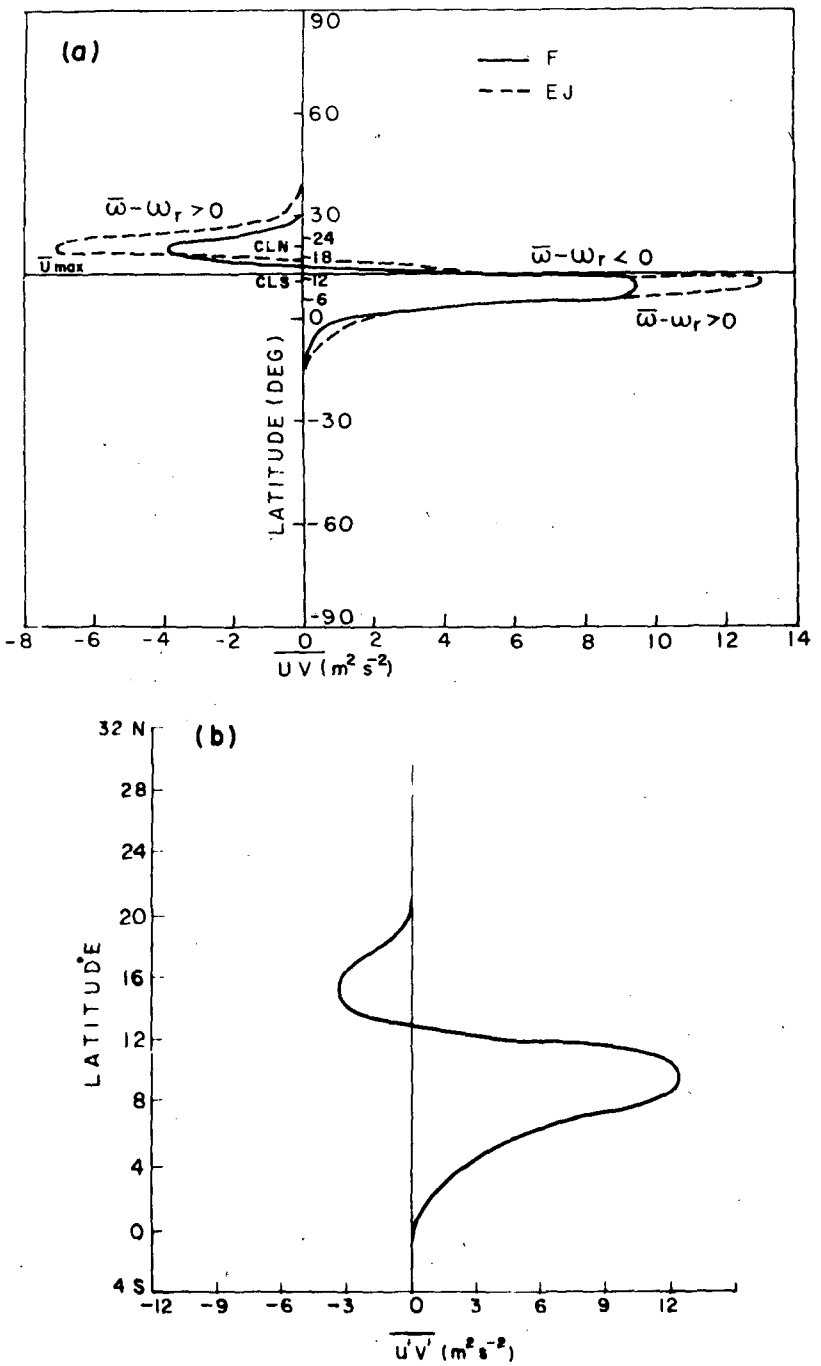

FIG. 6. Meridional profiles of (a) $\overline{UV}$ ($m^2 s^{-2}$) for the normalized divergent preferred wave on the sphere for the F and EJ basic states and (b) $\overline{u'v'}$ for the normalized divergent asymmetric preferred wave on the beta plane. The waves are normalized to the maximum meridional wind of 6 m s^{-1}. The lines marked as $\bar{u}_{max}$ indicates the location of the jet center.

This fact indicates that the instability is the manifestation of the wave overreflection at the critical latitudes. The wave is reflected from the extreme north and south turning points followed by a deep evanescent region. Further, the westerly angular momentum flux convergence is found to occur between the two critical latitudes. The angular momentum flux divergence is not seen to occur at the critical latitudes as expected from the theory in the limit $\omega_i \to 0$ (Lindzen and Tung, 1978). Thus, the absence of angular momentum flux

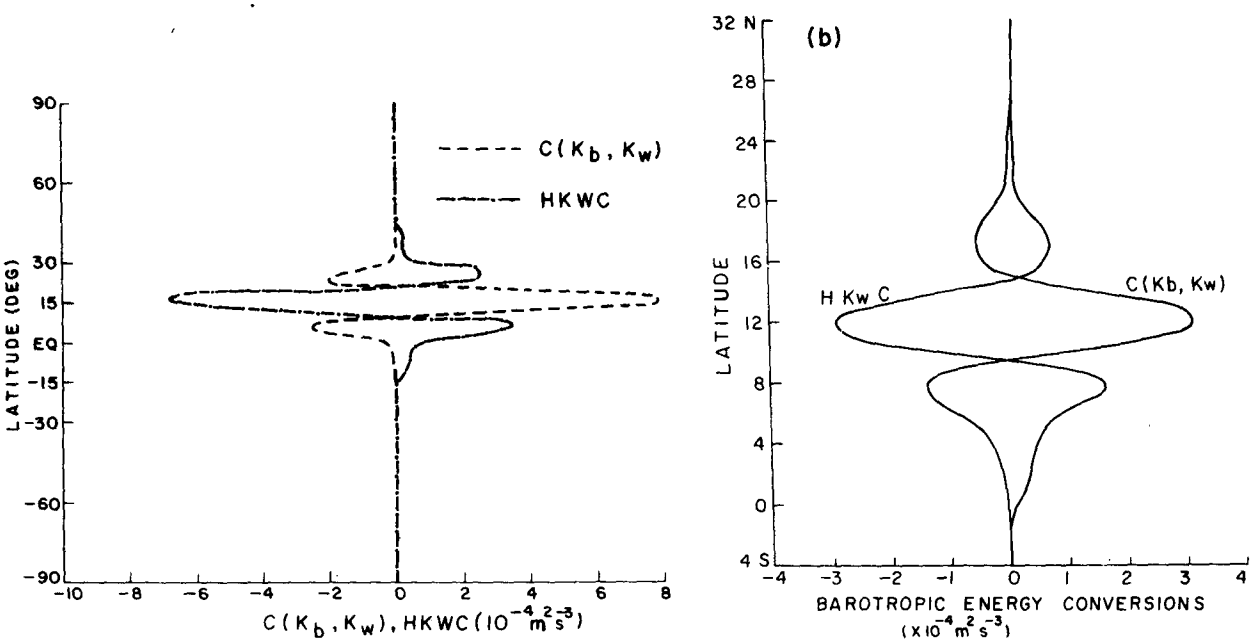

FIG. 7. Meridional profiles of barotropic energy conversion and the horizontal convergence (10^{-4} m^2 s^{-3}) of wave kinetic energy flux for (a) the normalized divergent preferred wave on the sphere for the EJ basic state and (b) the normalized divergent asymmetric preferred wave on the beta plane.

divergence at the critical latitudes can be attributed to the finite value of ω_i (Schoeberl and Lindzen, 1984).

Since the distance between the critical latitudes is nearly half of the distance between a critical and the nearest extreme turning latitude, it is expected that, in the instability, the overreflection of a wave between the two critical latitudes will dominate over the reflection of a wave between critical and turning latitudes. Lindzen and Tung (1978) have indicated that, if instability is due to the wave overreflection at a critical latitude, the growth rate can be estimated by means of the so-called laser formula. According to the formula, the growth rate is inversely proportional to the time taken by the wave to travel between the critical latitude and the energy-containing surface. In this study the two critical latitudes serve as the overreflecting and energy-containing surfaces. It may be inferred on the basis of these considerations that the growth rate will increase with the decrease of distance between the two critical latitudes. This conclusion can also be confirmed from results of the Schoeberl and Lindzen (1984) study on barotropic instability. Since the separation between the critical latitudes is more for the F profile than for the EJ profile, this explains qualitatively why the growth rates in the former case are less than in the latter case. It may be noted that more partial reflection is expected in the F case than in the EJ case because of the larger variations in the refractive index in the former case than in the latter case (Figs. 9a and 9b).

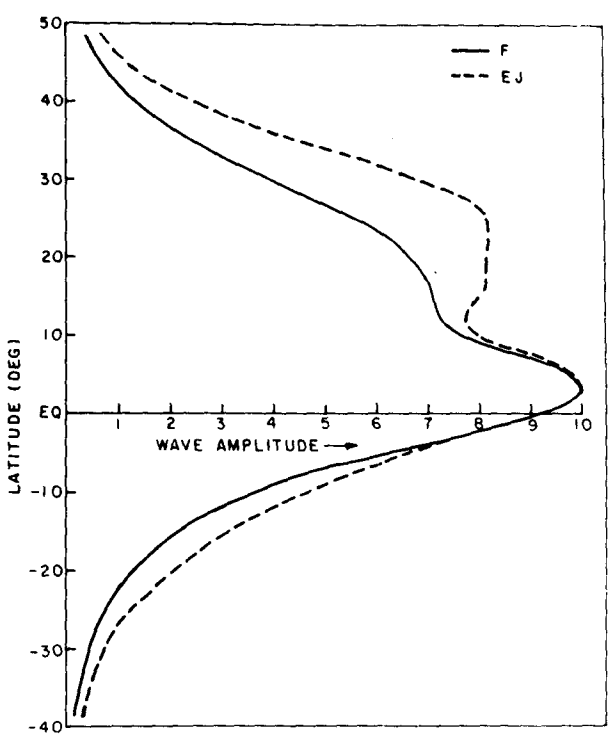

FIG. 8. Meridional profiles of amplitude (arbitrary unit) of the preferred wave for the F and EJ basic states.

It may be noted that the ratios of maximum northward westerly angular-momentum flux to maximum southward westerly angular-momentum flux are 2.5 and 1.9 for the F and EJ profiles, respectively. The angular momentum fluxes for the F case are closer to the observed values (Newell et al., 1972) than those for

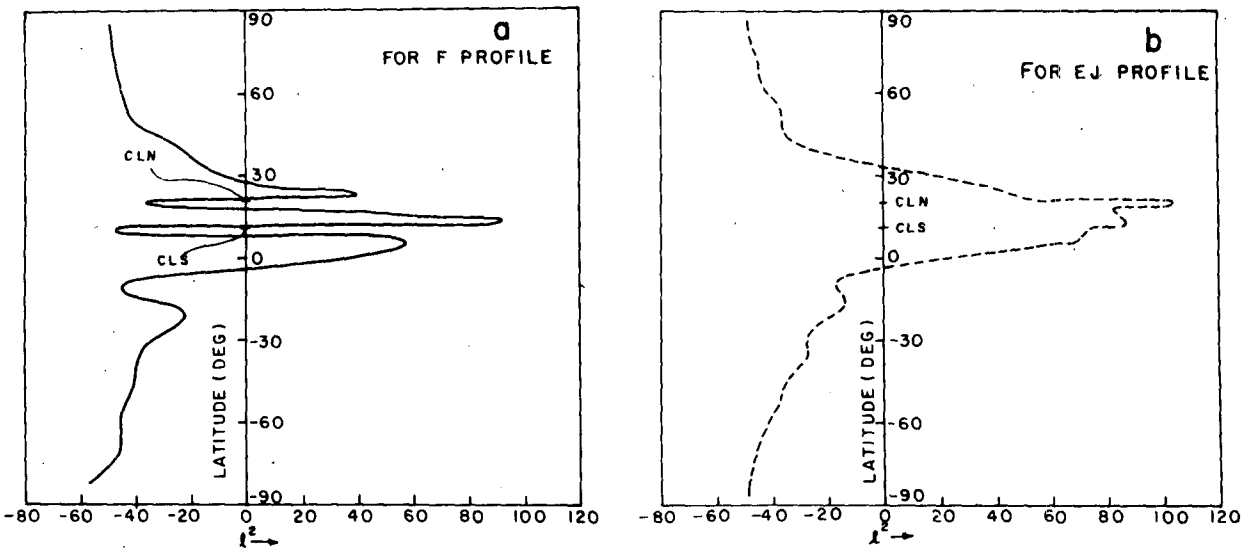

FIG. 9. Meridional profile of refractive index square (l^2) for wavenumber 7 for (a) the F and (b) the EJ basic states.

the EJ case. The angular momentum flux associated with the more unstable wave is larger than that of the less unstable wave.

6. Conclusions and discussion

The spherical geometry does not change significantly the zonal scale and the growth rate of the most unstable wave, and changes found in these properties can be attributed to the absence of lateral walls on the sphere.

The spherical geometry has a significant effect on the location of the wave amplitude maxima, displacing the primary maximum southward, closer to the equator. A strong correlation between the location of primary-wave amplitude maximum and the location of basic-state potential-vorticity gradient maximum to the south of the jet center has been noticed, which is similar to the result obtained on a beta plane. The location of secondary-wave amplitude maximum is strongly correlated to the location of basic-state potential vorticity minimum.

The spherical geometry has been found to play an important role in locating the maximum southward easterly angular-momentum transport generated by the most unstable wave, which is displaced to the north and is brought closer to the jet center in comparison to the beta-plane results. The location of maximum southward easterly angular-momentum transport coincides with the location of maximum meridional shear of $\bar{u}$. The energy source for the unstable wave is located in a narrow zone around the jet center, and away from this zone the energy for the wave growth is provided by the convergence of horizontal wave kinetic energy flux.

TABLE 1. Critical and turning latitudes for wavenumber 7.

Profiles	Critical latitudes	Turning latitudes
F	10.6°N, 20.45°N	3.95°S, 7.8°N, 10.9°N, 18.8°N, 21.2°N, 27.4°N
EJ	10.9°N, 20.55°N	3.55°S, 33°N

It has been shown that both midlatitude westerly jets inhibit the growth of disturbances along the easterly jet. The stabilizing influence of the westerly jets has been qualitatively explained in terms of the overreflection of meridionally propagating waves from critical latitudes coupled with a decrease of separation distance between the critical latitudes in their presence.

The f variation in the divergence term is neglected in this study. It is known that the f variation is maximum at the equator. If we assume that the f variation in the divergence term is more important, it is expected that the linear primitive-equation barotropic unstable modes, where the f variation in the divergence is allowed, will differ significantly, at least in the near-equatorial region, from the divergent barotropic modes. It was found that the differences between the two modes were particularly small in the near-equatorial region. It is relevant to note that the unstable waves have large amplitude close to the equator.

The main objective of this study was to bring out the special regional features of the tropical easterly jet. The regional instability characteristics of the easterly jet will be lost if we consider the global zonal average $\bar{u}$ profile for a stability analysis. Therefore, much physical significance should not be attached to the unstable planetary waves.

Acknowledgments. The author wishes to thank Smt. S. S. Desai for valuable help received in preparing the manuscript and Kum. S. M. Deshpande for typing. The author is grateful to the Director, Indian Institute

of Tropical Meteorology, for his encouragement and keen interest in this study, The author wishes to thank the anonymous reviewers for their helpful suggestions.

REFERENCES

Branstator, G., 1983: Horizontal energy propagation in a barotropic atmosphere with meridional and zonal structure. *J. Atmos. Sci.*, **40,** 1689–1708.

Chang, C. P., 1971: On the stability of low-latitude quasi-geostrophic flow on a conditionally unstable atmosphere. *J. Atmos. Sci.*, **28,** 270–274.

Charney, J. G., and P. G. Drazin, 1961: Propagation of planetary-scale disturbances from the lower into the upper troposphere. *J. Geophys. Res.*, **66,** 83–109.

Colton, D. E., 1973: Barotropic scale interaction in the tropical upper troposphere during the southern summer. *J. Atmos. Sci.*, **30,** 1287–1302.

Eliassen, E. B., B. Machenhauer and E. Rasmussen, 1970: On a numerical method for integration of the hydrodynamical equation with a spectral representation of the horizontal fields. Rep. No. 2, Institute of Theoretical Meteorology, Copenhagen University, 35 pp.

Hollingsworth, A., 1975: Baroclinic instability of a simple flow on the sphere. *Quart. J. Roy. Meteor. Soc.*, **101,** 495–528.

Kanamitsu, M., T. N. Krishnamurti and C. Depradine, 1972: On scale interactions in the tropics during northern summer. *J. Atmos. Sci.*, **29,** 698–706.

Krishnamurti, T. N., 1971: Observational study of the tropical upper tropospheric motion field during the Northern Hemisphere summer. *J. Appl. Meteor.*, **10,** 1066–1096.

Kuo, H. L., 1978: A two-layer model study of the combined barotropic and baroclinic instability in the tropics. *J. Atmos. Sci.*, **35,** 1840–1860.

Lindzen, R. S, and K. K. Tung, 1978: Wave overreflection and shear instability. *J. Atmos. Sci.*, **35,** 1626–1632.

Lipps, F. B., 1963: Stability of jets in a divergent barotropic fluid. *J. Atmos. Sci.*, **20,** 120–129.

Mak, M., and C. Y. Kao, 1982: An instability study of the onset vortex of the south-west monsoon, 1979. *Tellus,* **34,** 350–368.

Manabe, S., J. L. Holloway and H. M. Stone, 1970: Tropical circulation in a time-integration of a global model of the atmosphere. *J. Atmos. Sci.*, **27,** 580–613.

Mishra, S. K., 1981: On computational efficiency of a primitive equation barotropic hemispheric spectral model. *Beitr. Phys. Atmos.*, **54,** 72–85.

——, and P. S. Salvekar, 1980: Role of baroclinic instability in the development of monsoon disturbances. *J. Atmos. Sci.*, **37,** 383–394.

——, and M. K. Tandon, 1983: A combined barotropic–baroclinic instability study of the upper tropospheric tropical easterly jet. *J. Atmos. Sci.*, **40,** 2708–2723.

——, D. Subrahmanyam and M. K. Tandon, 1981: Divergent barotropic instability of the tropical asymmetric easterly jet. *J. Atmos. Sci.*, **38,** 2164–2171.

Moura, A. D., and P. H. Stone, 1976: The effect of spherical geometry on baroclinic instability. *J. Atmos. Sci.*, **33,** 602–616.

Newell, R. E., T. W. Kidson, D. G. Vincent and G. J. Boer, 1972: *The General Circulation of the Tropical Atmosphere and Interactions with Extra-tropical Latitudes.* Vol. I, MIT Press, 258 pp.

Orszag, S. A., 1970: Transform method for the calculation of vector coupled sums: Application to the spectral forms of the vorticity equation. *J. Atmos. Sci.*, **27,** 890–895.

Pedlosky, J., 1979: *Geophysical Fluid Dynamics.* Springer–Verlag. 624 pp.

Rayleigh, Lord, 1880: On the stability of certain fluid motions. *Scientific Papers, Vol. 1.* Dover, 474–487.

Robert, A. J., 1966: The integration of low order spectral form of the primitive meteorological equations. *J. Meteor. Soc. Japan,* **44,** 237–245.

Schoeberl, M. R., and R. S. Lindzen, 1984: A numerical simulation of barotropic instability. Part I. Wave mean flow interaction. *J. Atmos. Sci.*, **41,** 1368–1379.

Shrinivasan, V., 1960: Southwest monsoon rainfall in Gangetic west Bengal and its association with upper air flow patterns. *Indian J. Meteor. Geophys.*, **11,** 5–18.

Shukla, J., 1977: Barotropic–baroclinic instability of mean zonal wind during summer monsoon. *Pure Appl. Geophys.*, **115,** 1449–1462.

Simmons, A. J., and B. J. Hoskins, 1976: Baroclinic instability on the sphere: Normal modes of the primitive and quasi-geostrophic equations. *J. Atmos. Sci.*, **33,** 1454–1477.

Tupaz, J. B., R. T. Williams and C.-P. Chang, 1978: A numerical study of barotropic instability in a zonally varying easterly jet. *J. Atmos. Sci.*, **35,** 1263–1288.

Yamasaki, M., and M. Wada, 1972: Barotropic instability of an easterly zonal current. *J. Meteor. Soc. Japan,* **50,** 110–121.